DOI: 10.61782/fa.2023.0353

forum acusticum 2023

APPROACHES TO PIEZOELECTRIC MICROMACHINED MICROPHONE DESIGN: COMPARATIVE STUDY

Josué Esteves[1] **Libor Rufer**[2*] **Didace Ekeom**[3]
Martial Defoort[1] **Skandar Basrour**[1]
[1] Univ. Grenoble Alpes, CNRS, Grenoble INP, TIMA, 46 Av. Félix Viallet, F-38000 Grenoble, France
[2] ADT MEMS, 360 rue Taillefer, F-38140 Rives, France
[3] Microsonics, 39, rue des Granges Galand, F-37550 Saint Avertin, France

ABSTRACT

Nowadays, the most advanced micromachined microphones on the market are represented with structures using the capacitive coupling principle. Structures and performances of these micro-devices resemble their millimetric counterparts, which are typically used as measuring microphones. In the past decade, thanks to technological progress of the microelectronics industry, microphones using a piezoelectric transduction have been proposed by several teams. Such novel microphones exploit the piezoelectric effect of a thin layer of aluminum nitride, incorporated in their diaphragm structure. In these microphones fabricated with micromachining technology, no fixed electrode is necessary, unlike capacitive microphones. This specificity significantly simplifies both design and fabrication and opens the door for a new improvement of acoustic overload point as well as harsh environmental applications. In this paper, we present and compare two most promising approaches to piezoelectric micromachined microphone design. The first approach is developed by using a flat, circular diaphragm fixed around its perimeter, having the piezoelectric layer with its upper electrode in the vicinity of the clamped region. The other approach involves a square diaphragm cut in a way to create several cantilevers. Such a structure enables a more compliant diaphragm compared to the first approach.

[*] ***Corresponding author***: LiborRufer01@gmail.com

Keywords: *microphone, piezoelectric, MEMS, microsystem.*

1. INTRODUCTION

The field of micromachined microphones has seen significant advancements in recent years with the growing demand for miniaturization and high-performance sensing capabilities in various applications. Micro-electro-mechanical systems-based (MEMS) acoustic sensors have been focused for a long time by academic and industrial research teams. The first developments of micromachined microphones were enabled by the progress in material science, fabrication technologies, miniaturization, and sensor techniques. Examples of these preliminary steps are the invention of electret microphone [1] and a progress in silicon-based static pressure sensors [2]. Further developments of micromachined microphones have been conducted by many research teams and focused on the most common general approach using a diaphragm as an active microphone element converting the acoustic signal to the mechanical one, and then converting the mechanical signal to the electric one through known transduction principles. This effort resulted in the first microphones using piezoelectric [3], capacitive [4], and piezoresistive [5] couplings. Later, the FET (field effect transistor) microphone using a new principle, enabled only by silicon micromachining, was invented [6]. Finally, an optical microphone was described, in which a diaphragm and a rigid structure form an optical waveguide with the geometry and thus the transmission properties dependent on the

diaphragm deflections modify the intensity and the phase of the transmitting optical signal [7].

From these early demonstrated micromachined devices, a capacitive microphone has been adopted as the dominant microphone type for further development for several reasons. The first reason was its much lower noise floor compared to piezoelectric or piezoresistive microphones. Another reason was a straight applicability of currently used industrial fabrication technologies for its fabrication, with no requirement for additional structural layers or process steps. With strong industrial support, the micromachined capacitive microphone reached a commercial form after more than twenty years of incubation and became one of the most successful commercial MEMS products in the history of microsystem technology [8]. The continuing research of this kind of microphone resulted in key performance parameters such as sensitivity, signal to noise ratio, and distortion, meeting high requirements for microphones for mobile applications [9].

More recently, the availability of aluminum nitride (AlN) layers in industrial fabrication processes brought an increased interest into piezoelectric-based micromachined devices. The piezoelectric microphone structure, thanks to the absence of a fixed electrode, offers a unique advantage due to its fabrication simplicity. Compared to the capacitive microphone, the piezoelectric structure enables higher diaphragm excursions, limited only by its nonlinear behavior, and thus higher acoustic overload point (AOP). This feature has brought attention to industrial and aerospace applications working with extremely high acoustic levels. One of the first piezoelectric microphones designed for aeroacoustic applications reached AOP of 172 dB, which is substantially higher than in currently available typical micromachined capacitive microphones [10].

The piezoelectric coupling effect can be readily integrated to form cantilever-based sensing structures. These structures, used as acoustic sensors, are more sensitive compared to diaphragm-based sensors and allow high values of signal to noise ratio (SNR) [11]. One of the cantilever-based piezoelectric micromachined microphones commercially produced claims the SNR value of 68 dB, which was the highest value of all commercially available micromachined microphones [12].

In this paper, we compare and discuss the simulation results for piezoelectric microphones of both membrane and cantilever types. Section 2 presents the proposed fabrication process and the piezoelectric materials that are considered in the study. The modeling approaches are described in Section 3, and the optimization process is explained in Section 4. Finally, Section 5 overviews the obtained results.

2. MICROPHONE STRUCTURES

2.1 Mechanical body

The microphone performance is determined by the response of its mechanical structure while considering the neighboring acoustic elements. Depending on the fabrication technology used, the number and dimensions of each layer composing the structure will vary along with their material constants and associated stresses. Among these layers is a seed layer deposited for AlN growth (typically molybdenum). Although this layer is important both for technological reasons and for resulting electrical properties of the bottom electrode, we have not included it in this study for the sake of simplicity.

For the same reasons, motivated by our focus to compare the three selected microphone structures, we will simplify the stress conditions in the microphone structures. The residual stresses that have a strong influence on the structure final behavior are dependent on the conditions of each fabrication step and are known only in a relatively large interval of values. This fact presents a difficult obstacle for accurate simulation results. For this reason, we have decided to consider for our study the SoI (silicon on insulator) technology that can be optionally combined with a stress engineering aiming at stress compensation [13]. For our simulation, we have not considered residual stresses and we have supposed at this level the table material constants, which can be replaced with more accurate values obtained after the first fabrication step evaluation. On the other hand, we have verified that the stresses present in the microphone structure originating from the acoustic load are significantly lower than the materials tensile strengths.

Each sample presented in the case study is supposed to be fabricated from the basic wafer shown schematically in Fig. 1. This relatively simple structure consists of the SoI wafer with deposited piezoelectric and metallic layers. During the fabrication process of the microphone structure, the front side patterning is applied on the metallic and piezoelectric layers to form the microphone sensitive parts. These sensitive parts are formed by a sandwich composition in which the piezoelectric layer is placed between two electrodes. The top electrode is formed of a metallic layer, and in our study, we suppose that a silicon device layer serves as the bottom electrode. The microphone diaphragm will be obtained by the backside etching of the silicon handle layer and buried silicon oxide layer.

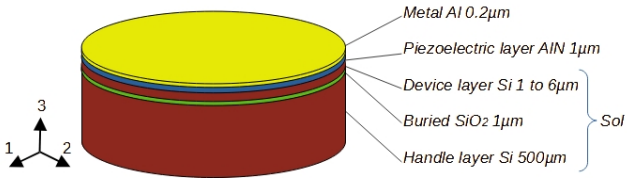

Figure 1. Basic wafer used for piezoelectric microphones fabrication.

In our study, we compare the simulation results of the three microphone structures (Fig. 2). The colors of structure layers used in Fig. 2 are identical to those described by the legend of Fig. 1. We firstly deal with a simple axisymmetric microphone (type A, Fig. 2a) with a circular diaphragm, as described in [10]. In another microphone structure (type B, Fig. 2b), the diaphragm is composed of four triangular cantilevers, obtained from a squared plate cut along its diagonals as firstly presented in [11]. Finally, our study is completed with a microphone structure (type C, Fig. 2c), having the diaphragm composed of four squared cantilever plates, as studied in [14]. There are two ways how these plates can be arranged to form a diaphragm. A simple solution, where two plates are clamped on one side of the diaphragm and the other two plates are clamped on the opposite side was repeatedly used by others. In our study, only one squared plate is clamped on each diaphragm side, which makes the overall diaphragm deformation more unified compared to a case where two plates are fixed on the opposite diaphragm sides. A drawback of this solution is discussed in the Paragraph 4.3.

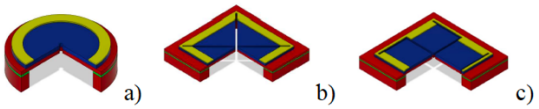

Figure 2. Mechanical structures used for the study shown schematically: axisymmetric microphone a), microphone with triangular cantilevers b), microphone with rectangular cantilevers c).

2.2 Piezoelectric layer

If we consider the main deformation of the piezoelectric layer obtained in all types of microphones shown in Fig. 2, the piezoelectric constitutive matrix equations, coupling the electrical and mechanical domains, can be reduced to the following equations:

$$S_1 = s^E_{11}T_1 + d_{31}E_3, \quad (1)$$

$$D_3 = d_{31}T_1 + \varepsilon^T_{33}E_3, \quad (2)$$

where S_1 and T_1 are mechanical strain and stress in axis 1, E_3 and D_3 are the electric field and the electric density displacement in axis 3, s^E_{11} is the component of the compliance matrix at constant electric field, d_{31} is the piezoelectric constant, and ε^T_{33} is the permittivity of the piezoelectric material at constant stress.

It has been shown, by using multi-criteria decision making (MCDM) material selection techniques, that from the currently available piezoelectric materials, AlN clearly stands out as the best candidate for the use as a microphone sensitive layer [15]. Aluminum nitride, followed by zinc oxide (ZnO) leads in quantitative parameters as low dielectric constant, low relative permittivity, high resistivity, low loss tangent, and high SNR value. Both, AlN and ZnO have good compatibility with complementary metal oxide semiconductor (CMOS) processing and good process quality control in manufacturing, which is important for device scaling and commercial applications. Tab. 1 summarizes the main material constants values of both passive and piezoelectric layers that were used in our work.

Table 1. Main material constants of the microphone layers.

	Si	SiO2	Al	AlN
Compliance s^E_{11} [TPa^{-1}]	7,67	13.7	14.3	3.57
Compliance s^E_{12} [TPa^{-1}]	-2,13	-2.33	-5	-0.98
Compliance s^E_{13} [TPa^{-1}]	-2,13	-2.33	-5	-0.9
Material density [kg/m^3]	2330	2200	2700	3260
Piezoel. const. d31[pm/V]	-	-	-	-2.646
Rel. permittivity ε^T_{33} [-]	-	-	-	8
Resistivity ρ [MΩm]	6x10^{-12}	10	2.7x10^{-14}	22.8

It can be noted that although isotropic materials are typically described with two engineering constants as Young's modulus and Poisson's ratio, we present the compliance matrix elements in order to keep uniformity of Tab. 1. We also present, for the reason of the compactness of Tab. 1, the electrical resistivity of all listed materials, although only that of AlN was used in simulations.

3. MICROPHONE MODELING

3.1 Finite-elements model

Our modeling relies mainly on two approaches, finite-element modeling (FEM), and lumped-element modeling (LEM). We have developed the finite-element model in the ANSYS Workbench ver. 2022 R1. With a proper definition of the boundary and symmetry conditions, we could model only a portion of the actual structure to reduce analysis run time and memory requirements with no losses in accuracy. Most of the simulations were done on one quarter of the structure (type A and C), and on ⅛ of the structure (type B). Structural layers (Si, SiO_2 and Al) are meshed with SOLID 186 elements, piezoelectric layer (AlN) is meshed with SOLID 226 elements allowing to define piezoelectric properties. Meshing size varies with the dimensions of the structure during the optimization process. Nevertheless, we prefer working with the linear lumped-element model towards the complete microphone evaluation for speed and availability purposes. FEM was thus an important tool to define the lumped elements with a high accuracy. It is briefly shown below how FEM was used to evaluate the nonlinear behavior of the microphone diaphragm. FEM enables also to verify the stress situation in the structure, predict the deformation and stress fields and must be considered in advanced design.

3.2 Lumped-element model

Lumped-element modeling is a powerful and reliable method for predicting the multiphysics behavior of electroacoustic transducers. With this method, each element of the transducer is transformed to a circuit model thanks to the mechanical (mass - damping - stiffness) and electrical (inductor - resistor - capacitor) equivalence. The use of this method requires characteristic lengths of the system smaller than the wavelength of the associated physical phenomena, which is satisfied in the audio-frequency range. In our case, we use the LEM shown on Fig. 3 already presented in [10]. This model allows evaluation of the microphone performance including its frequency range, sensitivity, noise, SNR, and minimum detectable pressure (MDP) values.

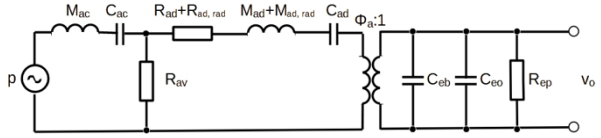

Figure 3. Lumped-element model of the piezoelectric microphone.

The model represents the mechanical elements transformed to its acoustic equivalents (resistance, mass and compliance of the diaphragm, R_{ad}, M_{ad}, C_{ad}), acoustic elements (diaphragm radiation mass and resistance, $M_{ad,rad}$, $R_{ad,rad}$, mass and compliance of the back cavity, M_{ac}, R_{ac}, and the pressure equalization vent resistance, R_{av}), and the electrical elements (sensing and parasitic capacitance, C_{eb}, C_{e0}, and resistance of the piezoelectric layer, R_{ep}). The acoustic pressure at the microphone input p is transformed to the output electrical voltage $v0$ with the transducer factor Φ_A. All these lumped elements can be obtained either from the FEM or analytically as was shown elsewhere [10, 16]. In this work, we focus on the presentation of the main microphone structures and the comparison of their performance parameters. Nevertheless, these parameters, such as the resonant frequency, the sensitivity, SNR, and AOP, which are well known in the field of acoustic sensors, are not presented here in detail as it is beyond the scope of this paper.

4. OPTIMIZATION

In piezoelectric microphones, the thickness, length, and width of all diaphragm layers, including the piezoelectric and electrode materials are key parameters that need to be optimized in the design loop. There are several optimal solutions satisfying the microphone specifications and widely used optimization algorithms often lead to trivial solutions. For this reason, we decided to apply a parametric optimization following Fig. 4. Our optimization process is performed in two computing environments (ANSYS and MATLAB) and involves two selection levels. The conditions No. 1 and 2, corresponding to both selection levels are chosen depending on the focused parameters of the specifications.

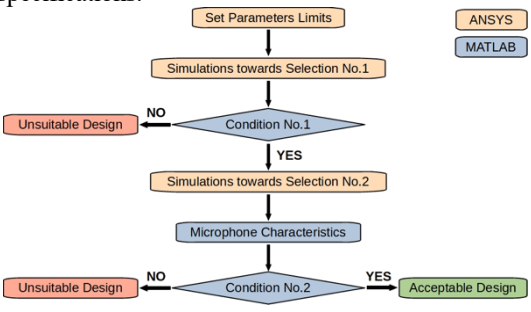

Figure 4. Optimization organizational chart.

4.1 Optimization towards the upper limiting frequency (ULF)

If we aim at the optimal design of a microphone matching a required frequency bandwidth, we set the limits for the structure dimensions and we run static and modal finite-element analyses (FEA). We filter the obtained results through the condition No. 1 of the optimization chart from Fig. 4. This condition is satisfied only by the solutions having the frequency of the first mode in a predefined range, which are related with the maximal frequency of the bandwidth. Number of suitable designs, depending on the range size defined for the first condition, passes back to ANSYS for the lumped elements extraction based on the static simulation, and then to MATLAB for the microphone characteristics evaluation. For the final step, the maximal value of the SNR is selected as the condition No. 2. The frequency response of the optimized geometry is then compared with electro-mechanical harmonic analysis from ANSYS.

4.2 Optimization towards the acoustic overload point (AOP)

If we look for a microphone withstanding a high acoustic pressure, we need to set the limits for the structure dimensions and to determine, through the nonlinear static analysis, the maximal diaphragm displacements for a given range of the input static pressures. Based on the deviation between the obtained value of the nonlinear displacement and the corresponding linear displacement, we obtain the acoustic overload point [10]. Fig. 5 shows that there is an important difference between the linear and the nonlinear displacement responses for the structure type A.

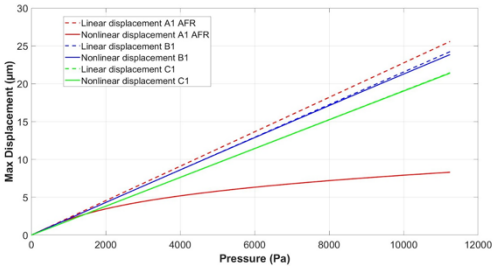

Figure 5. Maximal diaphragm displacement for the three microphone structures obtained in linear and nonlinear static FEA.

For this structure, we set the optimization condition No. 1 corresponding to the difference between the linear and the nonlinear displacement equal to 3 %. Each structure fulfilling the condition No. 1 for a predefined range of acoustic pressures passes towards selection No. 2. In this second step, the maximal value of the SNR is used as the condition No. 2.

Fig. 5 also documents that the microphone structures B and C, with the diaphragms composed of cantilevers, have almost linear behavior compared to the structure A. The same condition No. 1, which was used for the structure A, is not applicable to the structures B and C, as it leads to extremely large displacements. The optimization adapted to these cases is discussed in the following paragraph.

4.3 Optimization towards the low limiting frequency (LLF)

Microphone diaphragms composed of cantilever plates, as in the cases B and C, necessarily present slits between each of the plates. The width of the slits and the thickness of the diaphragm are sensitive parameters determining the pressure equalization resistance and thus the microphone lower limiting frequency. The effect of the slits width on the low-end roll-off of the microphone response is shown in Fig. 6a and Fig. 7a.

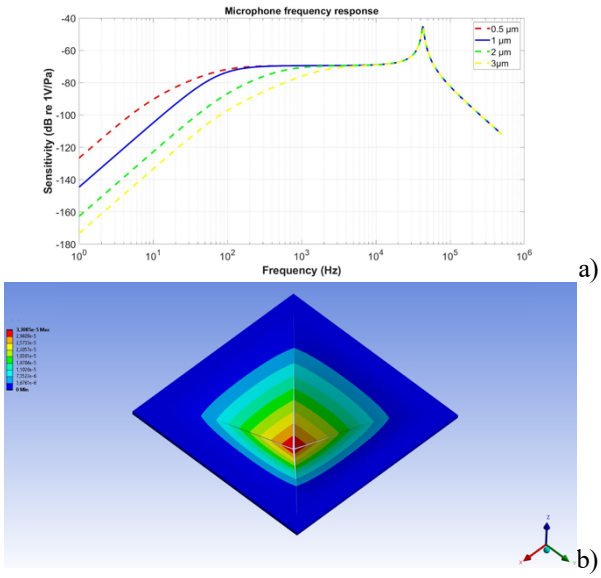

Figure 6. Microphone structure type B: Effect of the slits width on the low-frequency response a), Slits width during the deformation with the pressure obtained from the optimization AOP shown with the scale factor of 10 b).

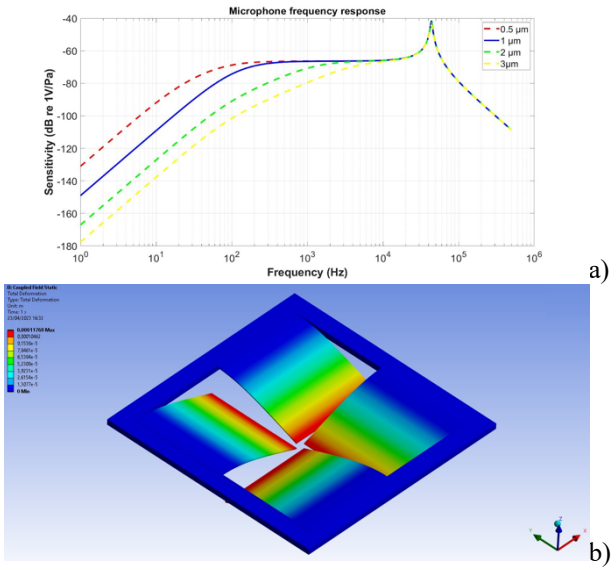

Figure 7. Microphone structure type C: Effect of the slits width on the low-frequency response a), Slits form during the deformation with the pressure obtained from the optimization AOP shown with the scale factor of 1 b).

These responses are valid for low acoustic pressures in which the width variation during the diaphragm excursion can be neglected. If the acoustic pressure increases, the induced diaphragm excursion is accompanied with an important slit deformation in the case of the structure B, as shown in Fig. 6b for the maximal pressure obtained following the Paragraph 4.2 (178 dB SPL). The slit effect could become more critical due to an important opening in the case of the structure C, as documented in Fig. 7b obtained also following the Paragraph 4.2 (190 dB SPL).
For this reason, in the case of the structures B and C, to avoid the acoustic short-circuit, or even a deterioration of the low-frequency end of the microphone response, we define the AOP value as the pressure generating the plate maximal excursion equal to its thickness. With such displacement limitation, we can suppose that the slits deformation due to the acoustic pressure approaching the AOP will be negligible and the microphone low-frequency response will not be affected.

5. CASE STUDY RESULTS

In this paragraph, we document the results of various cases studied in the microphone development.

5.1 Design towards the microphone sensitivity and SNR

We have performed the optimization of all three microphone structures focusing on the AOP value in the range of 160 to 175 dB for two configurations of the piezoelectric layer. In the first one, the piezoelectric layer was extended on the whole diaphragm surface, in the second configuration, the piezoelectric layer was localized only under top metallic electrode. For all three microphone types, the configuration with the piezoelectric layer fully covering the diaphragm surface was chosen for further development as more promising, especially in terms of the sensitivity and SNR. Nevertheless, it should be noted that the two cases with different piezoelectric layer coverage were issued from the optimization process, which kept the AOP in the required range. The dimensions of the resulting structures are necessarily not identical, which can also contribute to the difference in sensitivity. An example of this comparison is documented in Fig. 8 by the difference between the curves A1 and A2.
In the original optimization process, we kept the width of the sensitive layer on a constant value, based on preliminary simulations. In the next step, we have finely tuned the width of the electrode placed on the sensitive layer. An example of these results presents, in Fig. 8, the sensitivity and SNR as a function of the electrode width for the microphone type A. This analysis helps in the microphone design to fix the most important dimensions of its sensitive element.

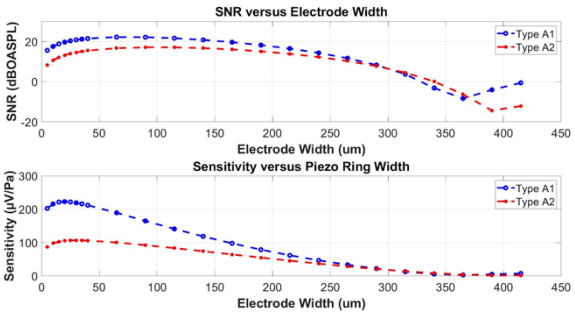

Figure 8. Effect of the electrode width on the microphone sensitivity and SNR with the piezoelectric layer fully covering the diaphragm (A1) or localized only under the electrode (A2).

5.2 Design for the audio bandwidth vs acoustic overload point

We have performed the optimization of all three microphone structures focusing on the audio frequency range and on the acoustic overload point. The comparison

of the optimized microphone parameters and performances is summarized in Tab. 2. The characteristics of the microphone structure A, optimized towards the acoustic overload point, are shown in the first column of Tab. 2. In this case, the condition No.1 of the optimization process was fixed by the range for the AOP level from 160 to 175 dB. The same structure A, optimized towards the resonant frequency in the range from 40 to 60 kHz is listed in the second column of Tab. 2. In this case, the AOP was obtained based on the requirement that the difference between the linear and the nonlinear displacement equals to 3 %, as described in Paragraph 4.2. We can notice differences in all parameters of Tab. 2 for these both application cases for the microphone structure A. The structure A/AOP leads with a higher AOP value, whereas the structure A/ULF is distinguished by its higher sensitivity and SNR.

Table 2. Comparison of the optimized microphones structures.

Mic / Optimization	A/AOP	A/ULF	B/ULF	C/ULF	B/ULF*	C/ULF*
Diaphragm diam. (side) [µm]	880	1276	1232	836	1760	1672
Silicon layer thickness [µm]	3	3	5	4	2	4
Piezoel. layer thickness [µm]	1	1	1	1	1	1
Electrode width [µm]	40	58	56	38	80	76
Back cavity volume [mm^3]	0.3	0.64	0.76	0.35	31	33
Resonant frequency [kHz]	88	45	43	44	10	10
Sensitivity [µV/Pa]	212	382	338	474	1855	2300
SNR A-weighted [dBA]	30	38	38	35	55	55
SNR@1kHz [dB]	64	72	72	69	89	89
AOP [dB]	163	149	163	161	127	138

As explained earlier, the optimization towards the AOP, as used for the structure A, is not applicable to the structures B and C. In these cases, we have used the optimization towards the upper frequency limit with the same condition for the resonant frequency in the range from 40 to 60 kHz as previously. For these two structures, B and C, the AOP was obtained as the imposed pressure on a diaphragm generating the maximal displacement equal to its thickness, as described in Paragraph 4.3.

We can notice that the first four microphone cases presented in Tab. 2 are characterized with relatively low values of the SNR presented, as usually, over the audible bandwidth with A-weighted values (dBA), including a correction factor corresponding to the human ear's frequency sensitivity in the range from 20 Hz to 20 kHz. This can be explained with a high noise, typical for piezoelectric transduction, accompanied with a low sensitivity resulting from dimensions dictated for required resonant frequency. For this reason, we also introduce here narrow-band values of the SNR at 1 kHz over a bandwidth of 1 Hz, which are more frequently used in aeronautics or in other industrial applications working with high-level acoustic fields [10].

Finally, in the effort to find a suitable microphone structure for speech applications, having a reasonable SNR value, we run the optimization towards the upper frequency limit as previously, but with the condition for the resonant frequency in the range from 10 to 15 kHz. To reach this frequency condition, the microphone stiffness must be much lower than in the previously presented cases, which needs not only to adapt the diaphragm dimensions, but also to significantly increase the microphone back cavity. Such a cavity increase may bring additional issues in the microphone design and implementation and can be a topic of an additional and independent study. As a result, we can see in the last two columns of Tab. 2 both simple cantilever-based structures, B and C with substantially improved SNR thanks to the increased diaphragm lateral dimensions and thus the sensitivity. Further improvement, which would go beyond the scope of this paper, can be obtained with optimal electrode locations and geometry [14, 17].

6. CONCLUSION

In this paper, we have presented the most promising structures for micromachined piezoelectric microphone

development. We have presented modeling and optimization approaches applied to these structures in view of two potential applications: 1. measurements of high-level acoustic fields, and 2. consumer applications in typical audio frequency range. It was shown, based on simulations, that all three studied microphone types are suitable for the audio applications and can be considered for high acoustic loads, but at the cost of relatively low values of the sensitivity and SNR. The microphone structures B and C can offer higher sensitivity and SNR values comparing to the structure A, but at the cost of limited frequency range.

7. ACKNOWLEDGMENTS

The results reported in this paper have been obtained with the support of the French Direction Générale de l'Aviation Civile via the project MAMBO (Méthodes Avancées pour la Modélisation du Bruit moteur et aviOn).

8. REFERENCES

[1] G. M. Sessler and J. E. West, "Self-Biased Condenser Microphone with High Capacitance", *Journal Acoust. Soc. Am.*, vol. 34, no. 11, pp. 1787-1788, 1962.

[2] S. Samaun, K. D. Wise, E. D. Nielsen, and J. B. Angel, "An IC Piezoresistive Pressure Sensor for Biomedical Instrumentation", *IEEE International Solid-state Circuits Conference*, (Univ. of Pennsylvania), pp. 104-105, 1971.

[3] M. Royer, P. Holmen, M. Wurm, P. Aadland, and M. Glenn, "ZnO on Si integrated acoustic sensor", *Sensors & Actuators*, vol. A, no. 4, pp. 357-362, 1983.

[4] D. Hohm and G. M. Sessler, "An integrated silicon-electret-condenser microphone", in *Proc. of the 11th Int. Congress on Acoustics*, (Paris, France), vol. 6, pp. 29-32, 1983.

[5] R. Schellin and G. Hess, "A silicon subminiature microphone based on piezoresistive polysilicon strain gauges", *Sensors & Actuators* vol. A: Physical, vol. 32, no. 1-3, pp. 555-559, 1992.

[6] W. Kühnel, "Silicon Condenser Microphone with Integrated Field-effect Transistor", *Sensors & Actuators*, vol. A, no. 25-27, pp. 521-525, 1991.

[7] U. Schneider and R. Schellin, "A phase-modulating microphone utilizing integrated optics and micromachining in silicon", *Sensors & Actuators*, vol. A, no. 41-42, pp. 695-698, 1994.

[8] P. V. Loeppert and S. B. Lee, "SiSonic TM – The First Commercialized MEMS Microphone", *Solid-State Sensors, Actuators, and Microsystems Workshop*, (Hilton Head Island, South Carolina, USA), pp. 27-30, 2006.

[9] A. Dehé, M. Wurzer, M. Füldner, and U. Krumbein, "Design of a Poly Silicon MEMS Microphone for High Signal-to-Noise Ratio", *Proc. of the European Solid-State Device Research Conference (ESSDERC)*, (Bucharest, Romania), pp. 292-295, 2014.

[10] M. D. Williams, B. A. Griffin, T. N. Reagan, J. R. Underbrink, and M. Sheplak, "An AlN MEMS Piezoelectric Microphone for Aeroacoustics Applications", *Journal of Microelectromechanical Systems*, vol. 21, no. 2, pp. 270-283, 2012.

[11] K. Grosh and R. J. Littrell, "Acoustic Transducer with Gap-controlling Geometry and Method of Manufacturing an Acoustic Transducer", *US Patent No. US 9,055,372 B2*, Jun. 9, 2015.

[12] S. Taranovich, "Vesper Piezoelectric MEMS Microphone with 68 dB SNR", *Electronic Design News (EDN) Product Review: www.edn.com/vesper-piezoelectric-mems-microphone-with-68-db-snr/*, 4 pp, 2015.

[13] E.Trioux, S. Monfray, T. Skotnicki, P. Muralt and S. Basrour "Fabrication of bilayer plate for a micro thermal energy harvester", *IEEE SENSORS 2014,* Valencia, Spain, pp. 2171-2174.

[14] Y. C. Chen, S. C. Lo, S. D. Wang, Y. J. Wang, M. Wu, and W. Fang, "On the PZT/Si unimorph cantilever design for the signal-to-noise ratio enhancement of piezoelectric MEMS microphone", *Journal of Micromech. Microeng.*, vol. 31, no. 105003, 16 pp, 2021.

[15] P. Gangidi, N. Gupta, "Optimal selection of dielectric film in piezoelectric MEMS microphone", *Microsystem Technologies*, vol. 25, pp. 4227-4235, 2019.

[16] J. Esteves, L. Rufer, D. Ekeom, S. Basrour, "Lumped-parameters equivalent circuit for condenser microphones modeling", *Journal Acoust. Soc. Am.*, vol. 142, no. 4, pp. 2121-2132, 2017.

[17] R. J. Littrell, K. Grosh, "Noise minimization in micromachined piezoelectric microphones", in *Proc. of the Int. Congress on Acoustics (ICA),* (Montreal, Canada), 9 pp., 2013.